Chemical Physics Letters 621 (2015) 171–176

Contents lists available at ScienceDirect

Chemical Physics Letters

journal homepage: www.elsevier.com/locate/cplett

Surface enhanced fluorescence from corroles and SERS studies of explosives using copper nanostructures

Syed Hamad [a], G. Krishna Podagatlapalli [b], Md. Ahamad Mohiddon [c], S. Venugopal Rao [b,*]

[a] School of Physics, University of Hyderabad, Prof. C. R. Rao Road, Hyderabad 500046, India
[b] Advanced Centre of Research in High Energy Materials (ACRHEM), University of Hyderabad, Prof. C. R. Rao Road, Hyderabad 500046, India
[c] Centre for Nanotechnology, University of Hyderabad, Prof. C. R. Rao Road, Hyderabad 500046, India

ARTICLE INFO

Article history:
Received 25 October 2014
In final form 5 January 2015
Available online 10 January 2015

ABSTRACT

We report the deployment of complex copper nanoparticles (NPs) and nanostructures (NSs), fabricated in a single step by ultrafast laser ablation of copper (Cu) in corroles/chloroform solutions, for surface enhanced fluorescence and surface enhanced Raman scattering studies (SERS). The characterization was performed by TEM, SAED, UV–visible absorption, and SEM techniques. Florescence enhancement of five orders in magnitude was obtained from corroles conjugated to Cu complex NPs. Cu NSs were utilized to record the SERS spectra of adsorbed Rhodamine 6G and explosive molecules of 5-amino-3-nitro-1,2,4-triazole and 1,1-diamino-2,2-dinitroethene. The estimated enhancement factors were in the range of 10^6–10^8.

1. Introduction

Over the last two decades plasmonic metal nanoparticles (NPs) have encountered potential applications in biotechnology [1], chemistry [2], and photonics [3,4] due to their outstanding optical properties. They have been proved to play a crucial role in realizing the true potential of surface enhanced Raman scattering (SERS) [5–14] and surface enhanced florescence (SEF) techniques [15–21]. In SERS technique any molecule in the vicinity of nanomaterial experiences the combined field of incident and local fields and, therefore, enhances the macroscopic polarization of molecular medium. This phenomenon is termed as electromagnetic enhancement [22–24]. Efficient SERS necessitates the close contact between analytes and metal NP surface which, typically, is 20–30 Å [25]. At these distances, fluorescence of analytes is extensively quenched and minor enhancements have been observed than those obtained in SERS. When the analytes are placed in the vicinity of NPs (>50 Å) enhancement in the fluorescence is significantly orders of magnitude higher, which is referred to as surface enhanced fluorescence (SEF) [26]. SEF has been extensively utilized as an efficient tool for imaging and detection in the fields of life sciences and chemical sciences by improving the quantum yield, excitation rates of fluorophore [27]. The predominant reason behind SEF is enhanced local fields in the proximity of fluorophore which in turn amplifies the radiative decays and their quantum yields [18]. The effect of plasmons on fluorophore depends on the shape, size, and chemical composition of the metal NPs. Thus far SEF studies were focused on fluorophores attached to noble metal films such as silver and gold NPs which were fabricated by different physical and chemical methods and obtained significant enhancements of fluorescence intensity [28–31]. Cu nanomaterials have not been studied effectually for SEF since the absorption cross-section depends on the imaginary component of dielectric function [Cu (5.8), Ag (1.66) and Au (1.86)] exhibiting an absorption maximum near 560 nm [32]. Due to this, the possibility of fluorescence quenching by Cu NMs prevails because the emission band of most analytes are in the 560–740 nm region. We have achieved an absorption band of Cu NPs near 400 nm (from 580 nm) through ultrafast laser ablation (ULAL) of Cu NPs in chloroform [3,33]. This is due to direct adsorption of Cl^- ions on metal NPs those originate from solvent disintegration through laser ablation [3,33]. It was also reported that the characteristic absorption band of ns (532 nm) and fs (800 nm) laser generated Au NPs in chloroform appeared in the UV region [34]. Mortier et al. [35] accomplished the SPR band near 565 nm for Au NPs fabricated with ns pulses. Karolína et al. [36] demonstrated UV region characteristic absorption bands for Au NPs in chloroform and 5,10,15,20-tetrakis-4-pyridylporphine (TPyP). Our earlier studies suggested that spherical chlorinated Cu NPs achieved in chloroform using ~2 ps pulses depicted absorption band in the 370–390 nm region and cubical NPs demonstrated absorption bands in UV/visible region [33]. Additionally, nano-/micro-structures on Cu substrate were observed in the same

* Corresponding author.
E-mail address: svrsp@uohyd.ernet.in (S. Venugopal Rao).

http://dx.doi.org/10.1016/j.cplett.2015.01.006
0009-2614/

experiment. The fabrication of Cu NPs/NSs in liquids using ULAL has demonstrated nanomaterials with low cost, stability, high reproducibility as platforms for huge electric field enhancements when used as SERS substrates for detecting explosives [37–39] such as 5-amino-3-nitro-1,2,4-triazole (ANTA), trinitrotoluene (TNT), 1,3,5-trinitroperhydro-1,3,5-triazine (RDX) and 1,1-diamino-2,2-dinitroethene (FOX-7) etc.

Corroles have been preferred for our studies because they are tetra pyrrolic organic molecules and generally demonstrate porphyrin type spectra [40], with strong absorption in the visible region. Moreover, the pyrole–pyrole linkage appears to provide strong fluorescence properties in corroles than the porphyrin counter parts [40,41]. Corroles have potential in real time applications such as cancer diagnostics, optical limiting, solar cells and photonics [41]. In this letter, we demonstrate(a) fabrication of Cu colloids in diluted triphenyle corrole (TPC) and tritolyl corrole (TTC) chloroform solutions (25 μM) using ULAL method (b) fabrication of stable chlorinated Cu NP by ablating pure copper targets in

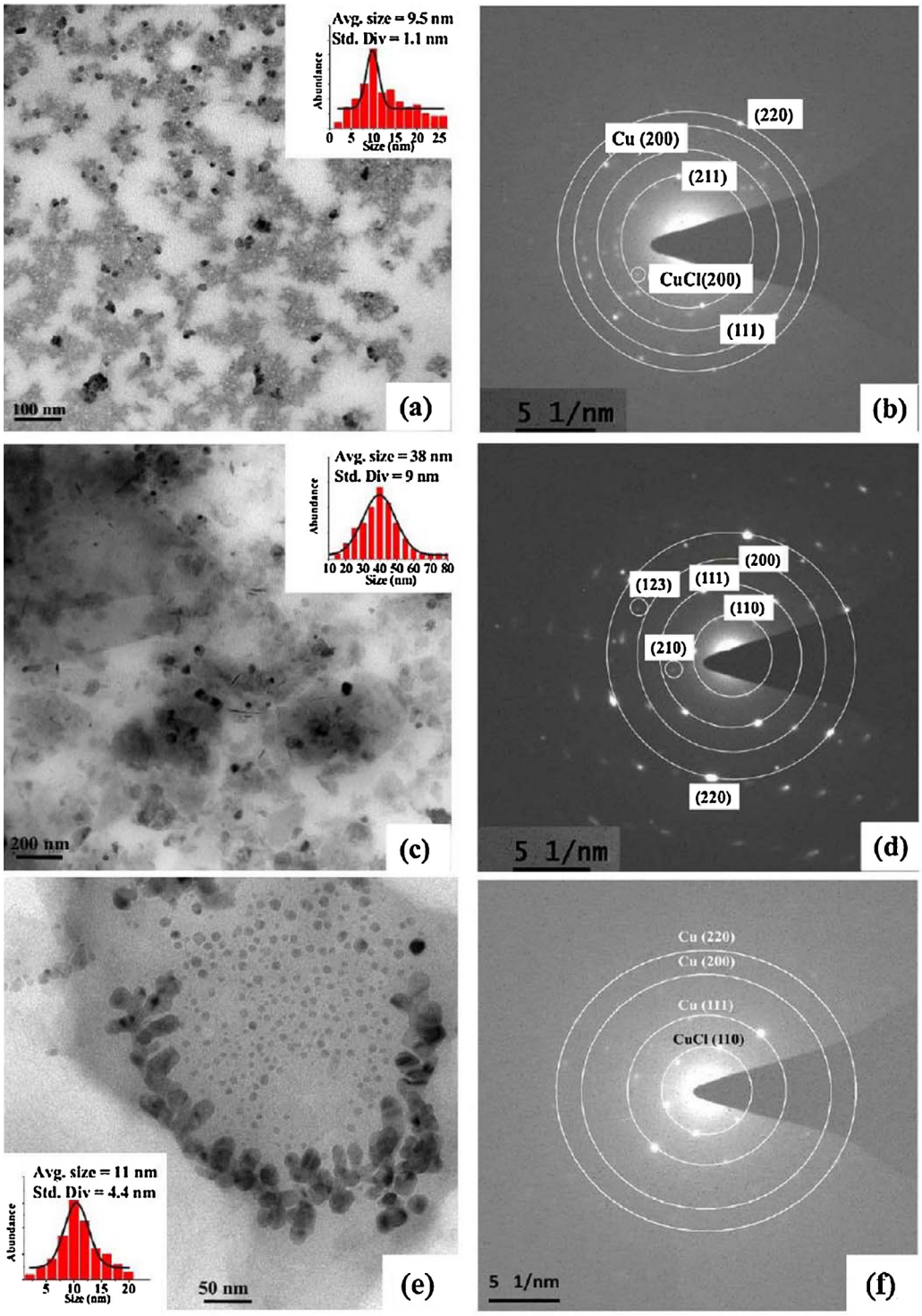

Figure 1. TEM micrographs of corrole/Cu colloids prepared in liquid media: (a) NP1 in TTC, (c) NP2 in TPC and (e) NP3 in chloroform. Insets of (a), (c), and (e) illustrate the size distribution. (b), (d) and (e) SAED patterns of NP1 in TTC, NP2 in TPC and NP3 in chloroform.

chloroform (c) significant orders of magnitude enhancement in SEF from chlorinated Cu NPs in corrole solutions and SEF studies of TTC and TPC using Cu/CuCl nanocomposites fabricated in chloroform (d) SERS measurements of Rhodamine 6G and explosive molecules (ANTA and Fox-7) with significant enhancement factors (E.F.'s). Structural, spectroscopy details of the corroles used in this study are reported elsewhere [41,42].

2. Experiments

Complete details of ULAL were reported in our earlier works [3,4]. In this study Cu targets were ablated in chloroform and in diluted TPC, TTC (2.5×10^{-5} M) solutions. Briefly, Cu metal target is placed at the bottom of Pyrex cell filled with liquid. Typical height of the liquid above the surface of target was ~5 mm. The spotsize on the sample surface was ~90 μm. Typical fluence of ~2.5 J/cm^2 and an ablation time of 30 min were used. Earlier to this study, we had performed a series of experiments [3,33,37] to estimate the appropriate fluence for liquids to be utilized in these experiments. Our studies clearly demonstrated that the fluence of ~2.5 J/cm^2 (>ablation threshold fluence of Cu, 2 J/cm^2) was optimal for producing better yields along with finer dimensional nanoparticles. The liquid filled Pyrex cell with Cu target was placed on motorized *X*–*Y* stages. The stages were translated to draw periodic lines on Cu target at separation of ~60 μm. The shape/size of NPs and absorption were characterized by TEM, UV–visible spectroscopy, respectively. Crystallographic phases and composition of fabricated NPs was confirmed by selective area electron diffraction pattern (SAED).

3. Results and discussion

To avoid ambiguity, the fabricated Cu colloids in TTC, TPC and pure chloroform are labelled as NP1, NP2 and NP3, respectively. Figure 1(a), (c) illustrate the TEM images of NP1, NP2 and insets show the size distribution. It was observed that the morphologies of fabricated NPs were spherical in nature. Following a Gaussian fit of the size distribution histogram; average sizes of the NPs were found to be ~9.5 nm and ~38 nm in NP1 and NP2, respectively. Figure 1(b), (d) illustrate the SAED spectrum of NP1 and NP2, respectively. The shape of SAED pattern revealed that the particles were nanocrystalline in structure and the measured inter planar separations (d) for NP1 were 3.2 Å and 2.6 Å, in agreement with those of copper chloride (CuCl) crystal planes [(2 0 0), and (2 1 1)] and 2.2 Å, 1.82 Å and 1.28 Å matching with Cu (1 1 1), (2 0 0) and (2 2 0) planes. In the case of NP2, '*d*' values were 4.6 Å, 2.8 Å, 1.7 Å in good agreement with the CuCl planes of (1 1 0), (2 1 0), (1 2 3), and the atomic spacing values of 2.19 Å, 1.81 Å, and 1.36 Å were in good agreement with Cu crystal planes of (1 1 1), (2 0 0), and (2 2 0). SAED results revealed that Cu NPs and CuCl NPs were formed in the colloidal solutions. The average sizes of NPs were similar in the case of NP1 and NP3 (~9.5 and ~11 nm). However, NP2 demonstrated an average size of ~38 nm probably due to (a) aggregation effects (b) molecule–nanoparticle interaction being different in this case (c) slender differences in the experimental conditions such as input pulse chirp and/or pulse-to-pulse intensity variations, liquid level above target in each case, focusing exactly on the target, etc. Therefore, further detailed studies are essential for identifying the exact reason(s) behind the varying size of NPs. Similarly, from the TEM images of NP3 presented in Figure 1(e) it is evident that majority of produced NPs were smaller in size with a few NPs with large dimensions. The size reduction of NPs in NP3 case could be attributed to photo-fragmentation effect. The mean diameter of small particles, evaluated by Gaussian fit, was ~11 nm [inset of Figure 1(e)]. Similarly, the estimated average size of NPs with larger dimensions was

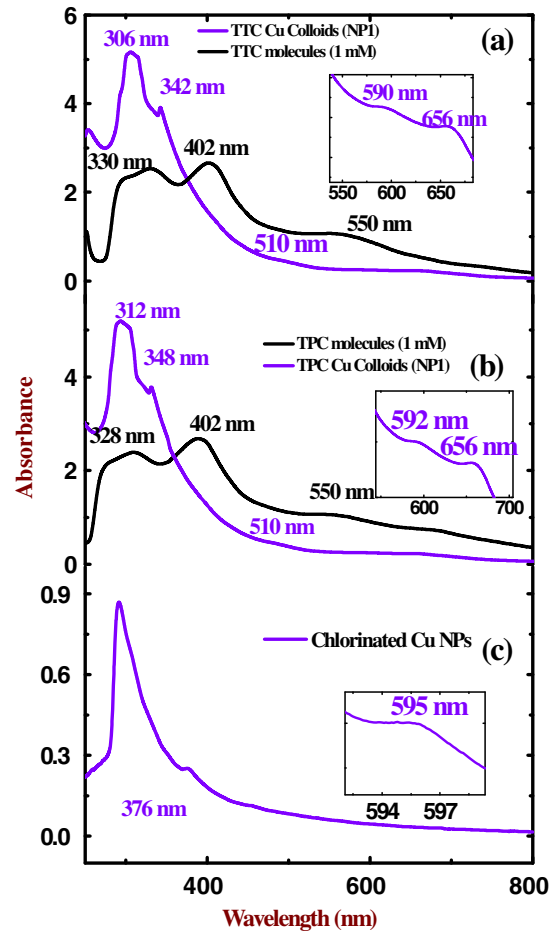

Figure 2. UV–vis absorption spectra of colloidal corrole and chlorinated Cu NPs (a) TTC (NP1) (b) TPC (NP2) and (c) chloroform (NP3).

~25 nm. Figure 1(f) illustrates SAED pattern of NP3 and it is evident that NP-3 phase was nanocrystalline. The ring pattern in SAED was indexed with cubic phase of CuCl crystal planes, which were confirmed from the measured inter-planar spacing (estimated from the diameter of rings in SAED image). The prevalence of CuCl (1 1 0) with '*d*' spacing of 4.5 Å and Cu (1 1 1), (2 0 0), and (2 2 0), with corresponding '*d*' spacing values of 2.18 Å, 1.81 Å and 1.29 Å, respectively, confirmed the formation of cubic phase for both Cu and CuCl NPs.

Figure 2(a), (b) illustrate the UV–visible absorption spectra of both NP1 and NP2 colloidal solutions. The spectra demonstrated a small SPR peak near ~590 nm in both the cases of NP1 and NP2. These small humps in the spectra confirmed the presence of Cu NPs. Moreover, the characteristic absorption peak observed near 350 nm in both the cases (NP1 and NP2) corresponds to the formation of CuCl NPs. The presence of chloride ion near Cu metal incites charge transfer between metal and the associated ligands leading to a shift of characteristic absorption peak to the UV region. Similar characteristic peaks of copper chloride NPs have been reported recently by our group [3,33]. One more peak was observed in the UV-region (near 300 nm) which is assigned to the metal inter-band transitions. This could be due to the reactivity of copper with atmospheric oxygen forming products such as copper oxide and hydroxide. The other, broad absorption peak near 656 nm confirmed that corrole molecules have not been damaged due to laser ablation. However, the characteristic peak of corrole molecule near 550 nm was blue shifted to 510 nm which, probably, could be due to the formation of corrole radicals [36]. Figure 2(c) illustrates the absorption spectra of NP3 and the absorption band obtained in UV-region was near

376 nm. There was also a small absorption band observed near 594 nm confirming the presence of Cu NPs in NP3. The presence of a band in the UV/visible region and yellow colouration of the samples suggest the formation of Cu/CuCl nanocomposites and CuCl NPs. Even though Cu belongs to plasmonic class of metals, the strength of surface plasmon resonances and corresponding absorptions are weak compared to Ag and Au. We strongly believe that during ablation process a sandwich type of material such as $TTC^{-2}/Cu^{+3}/Cl^{-}$ (or) $TPC^{-2}/Cu^{+3}/Cl^{-}$ could have been produced on the surface of Cu NP and finally TTC–Cu–Cl and TPC–Cu–Cl colloidal solutions were formed in NP1 and NP2, respectively [36]. The provisional interaction of short-lived metallic plume with Cl ions in the surrounding chloroform environment at the time of ablation results in CuCl NPs and Cu NPs in small amounts. One possible confirmation of the generation of sandwich type NPs was the recorded UV–vis absorption spectra exhibiting the characteristic peaks pertaining to Cu, chlorine, and Corroles. Whereas in the case of NP3 there could be formation of CuCl layer on the surface of Cu NPs permitting the formation of Cu/CuCl nanocomposites and the characteristic band of CuCl layer overwhelmed the absorption band in the SPR region.

SEF spectra have been recorded using micro-Raman spectrometer (WiTec-300 alpha) with 532 nm excitation source and spectra were collected through a CCD camera. The laser beam was focused on analytes placed on Cu substrates using microscopic objective [100 X, NA = 0.9] and back scattered signal was collected through the same objective. Two types of SEF measurements have been performed. A tiny drop (~10 μL) of (a) manually mixed corroles solution (1 nM) and chlorinated Cu NPs and (b) colloidal corrole Cu NPs were deposited on the cover slips. Three SEF spectra were recorded at different positions on the substrate and an average of the 3 spectra obtained was considered for analysis. Typical acquisition time used was 5 s. Figure 3(a) and (b) demonstrates the SEF spectra from NP1 and NP2, respectively. The enhancements were estimated by comparing with characteristic bands obtained in normal fluorescence spectra (NFS) of TTC (100 μM) and TPC (100 μM) at higher concentrations. Comparison of SEF and NFS of both TTC and TPC revealed that the intensity of fluorescence band in SEF spectra was enhanced by 13 and 333 times, respectively. Evidently, similar bands appeared in SEF (622 nm for TTC and 646 nm for TPC) spectrum and NFS as well. We did not observe any visible peak shift in SEF spectra compared to the peaks in NFS. A tiny drop (~10 μL) of manually mixed solution of corroles (1×10^{-9} M) and Cu/CuCl NPs in chloroform was placed on the glass slide and dried. Recorded SEF spectra of these dried samples are shown in Figure 3(c) and (d). The spectra illustrated very high intensity at 626 nm and 645 nm for TTC and TPC, respectively. SEF spectra of lower concentration (10^{-9} M) analytes (TTC and TPC) were compared with the higher concentration (1×10^{-4} M) spectra to estimate the E.F.'s and were found to be ~2.7×10^5 and ~7.1×10^5 for TTC and TPC, respectively. Fluorescence enhancements in the present case, possibly, occur due to (a) electromagnetic mechanism which motivates the amplification of incident field through excitation of surface plasmons (b) increase of quantum yield and radiative decay rates. In the first case of TTC–Cu–Cl and TPC–Cu–Cl colloidal solutions, fluorophores (TTC and TTC) were strongly adsorbed on metal surfaces inciting the fluorescence quenching [26,43]. Moreover, re-absorption of the fluorescence emission could have occurred through the attached Cu NPs whose SPR band falls in the range of fluorescence band of fluorophore [26]. Due to the re-absorption, fluorescence might have quenched significantly. In the second case, fluorophores (TTC and

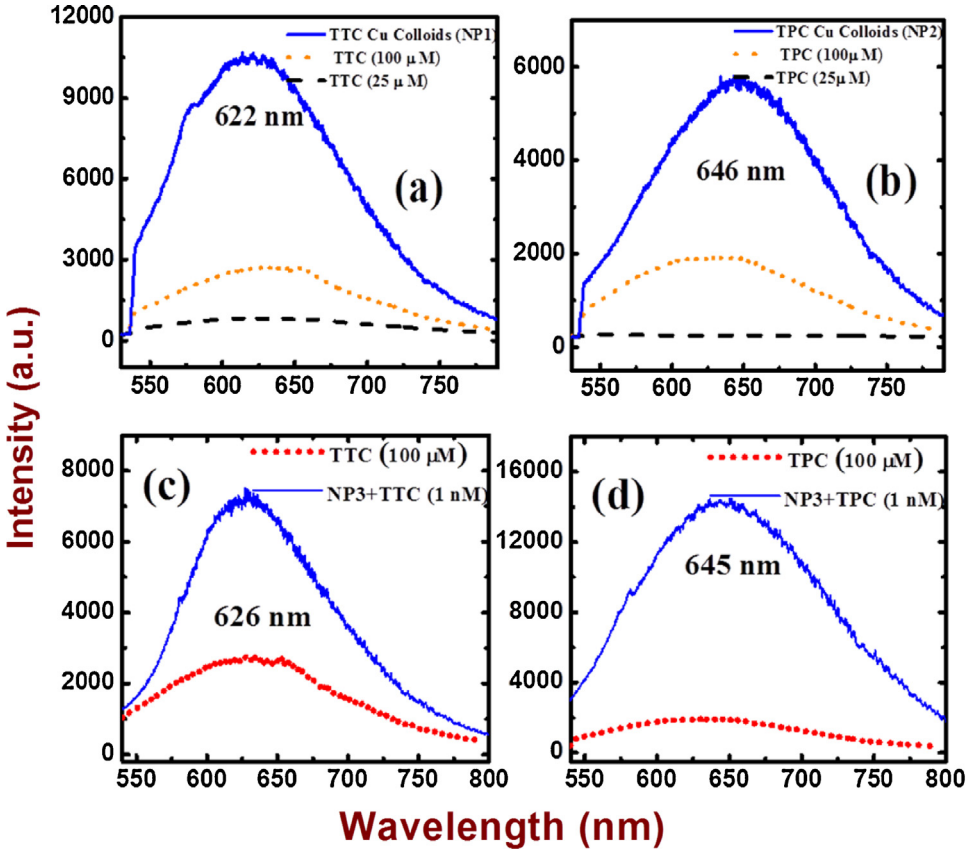

Figure 3. SEF spectra recorded from (a) TTC Cu Colloids (NP1) and (b) TPC Cu colloids (NP2). TTC (100 μM) and TPC (25 μM) spectra are represented by orange/dotted line and black/dashed line, respectively. The spectrum of NP1 (NP2) is represented by blue/solid line. SEF spectra recorded from (c) TTC and (d) TPC corroles adsorbed on NP3 individually. TTC (TPC) spectra are represented by red/dotted lines and TTC/TPC + NP3 by blue/solid lines. The integration time used was 5 s. (For interpretation of the references to color in figure legend, the reader is referred to the web version of the article.)

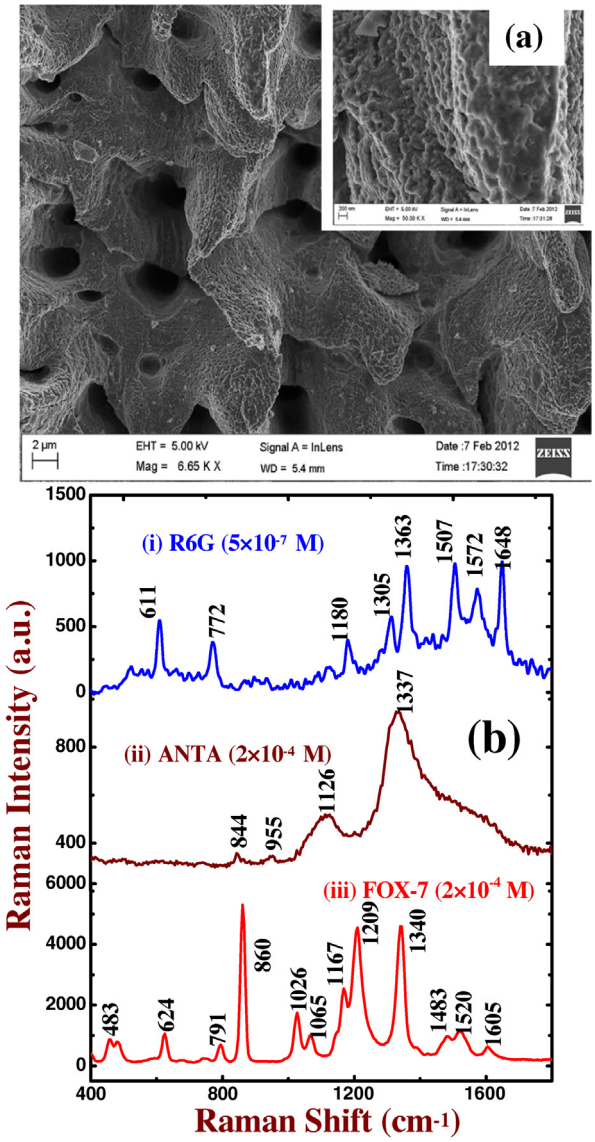

Figure 4. (a) FESEM image of NS's on the Cu substrate prepared in chloroform and (b) SERS spectra recorded from (i) R6G (blue/top – 5×10^{-7} M) (ii) ANTA (wine/middle – 2×10^{-4} M) and (iii) FOX-7 (red/bottom – 2×10^{-4} M) adsorbed on Cu NSs. (For interpretation of the references to color in figure legend, the reader is referred to the web version of the article.)

TPC) might not completely get attached to the Cu NPs surface since it was a passive mixing of CuNPs to TTC and TPC. In this case, due to the local field effect [43] of Cu NPs which were in the proximity of fluorophores, significant fluorescence enhancement was observed with very minimal quenching of fluorescence [26,43]. Furthermore, re-absorption of fluorescence emission band by the Cu NPs in the neighbourhood was possibly inhibited since their surface was passivated by CuCl layer.

Morphologies of the Cu NSs in chloroform are shown in Figure 4(a). The FESEM images demonstrated random nanostructures with typical size of ~100 nm. Magnified image depicts the formation of micron sized structures with sharp edges. Surface activity of Cu NS was investigated by recording the Raman spectra of three adsorbed molecules [R6G (1×10^{-9} M and 5×10^{-7} M), ANTA (1×10^{-6} M and 2×10^{-4} M), FOX-7 (1×10^{-6} M and 2×10^{-4} M)] on the Cu NS. The Raman spectra were recorded at 532 nm with a 0.9 NA objective. SERS spectra of R6G (1×10^{-9} M and 5×10^{-7} M) were recorded with 10–20 µL deposited on Cu NS to form a monolayer. An average spectrum of 10 spectra collected is illustrated in Figure 4(b)-(i) (top). E.F.'s were evaluated [44,45] by the comparing SERS spectra with normal Raman spectra of R6G deposited on plane silicon surface for the prominent peak at 1363 cm^{-1} corresponding to in plane aromatic C—C stretch. Enhancement factors were estimated using the procedure listed and SERS spectra R6G at 1×10^{-9} M concentration was shown in Figure 2(a) in SI.

In the case of R6G, at 1×10^{-9} M and 5×10^{-7} M concentrations the absorbed molecules (~35% and ~43%) on Cu NS were estimated by following a process reported earlier [37]. The estimated E.F.'s for the 1363 cm^{-1} mode were ~6×10^{8} and ~1.8×10^{7} for 1×10^{-9} M and 5×10^{-7} M concentrations, respectively. Assignments of other spectral modes are presented in SI. Large enhancement in the case of R6G could be due to the rough edges arising from micron sized structures on Cu surface. Later, the substrate was cleaned by sonication in acetone for 30 min and dried at room temperature. After two weeks, the same Cu substrate was utilized again for recording the SERS spectra of an explosive molecule (ANTA) at 1×10^{-6} M and 2×10^{-4} M concentrations. Figure 4(b)–(ii) (middle) illustrates the SERS spectra of ANTA adsorbed on Cu NSs. The spectral modes of ANTA [46] have been observed with lower intensity at 1×10^{-6} M in the Raman spectrum. The vibrational modes were observed at 533 cm^{-1} and 615 cm^{-1} associated with NH_2 deformation and NO_2 deformation, respectively. The main characteristic mode detected at 1337 cm^{-1} with lower intensity along with 1577 cm^{-1} mode assigned to C—NO_2 symmetrical stretch and C—NH_2 symmetrical stretch + NH_2 bend, respectively. For 2×10^{-4} M concentration the characteristic mode at 1337 cm^{-1} was elevated with good signal to noise ratio and few more modes were detected at 844 cm^{-1}, 955 cm^{-1} and 1126 cm^{-1}, which were not observed in SERS spectra at 1×10^{-6} M [see Figure 2(b) in SI] concentration. It was also observed that modes at 533 cm^{-1}, 615 cm^{-1} and 1577 cm^{-1} were not elevated clearly in the present case. It should be noted that no modes were observed in normal Raman spectra of ANTA (0.2 M, see SI). We estimated that ~47% and ~50% ANTA molecules were adsorbed on the NS substrate [37] for the concentrations of 1×10^{-6} M and 2×10^{-4} M, respectively. The evaluated E.F.'s for the 1337 cm^{-1} mode were ~1.4×10^{7} and ~2.8×10^{5} at 1×10^{-6} M and 2×10^{-4} M concentrations, respectively. Assignments of other spectral modes of both concentrations are summarized in Table 2 presented in SI. One day later, the SERS spectra of another explosive molecule (FOX-7) was recorded for third time after appropriate cleaning. Figure 4(b)-(iii) (bottom) illustrates the SERS spectra of FOX-7 and it depicts the characteristic Raman bands [47] corresponding to symmetric C—NO_2 stretching and NH wagging at 1340 cm^{-1} with lower intensity at a concentration of 1×10^{-6} M [see Figure 2(c) in SI] whereas the mode intensity was clearly enhanced at 2×10^{-4} M concentration. Moreover, the mode at 1483 cm^{-1} corresponding to out of layer symmetric NH wagging (NO and NH rocking), was observed in both cases. The calculated E.F.'s for the 1340 cm^{-1} mode were ~2.5×10^{5} and ~4.2×10^{4} for 1×10^{-6} M and 2×10^{-4} M concentrations, respectively. Assignments of other modes are presented in SI (Table 3).

The rough edges on Cu substrate demonstrated larger enhancements in R6G compared to ANTA and FOX-7. We believe that the following arguments support our observations (a) the dimensions of explosive molecules are smaller than R6G molecules and these molecules might not have electromagnetically attached to rough edged Cu structures appropriately. This suggests that rough edged Cu structure was not compatible to generate sufficient local fields which invoke electric dipoles vibrations and, therefore, resulted in lower enhancements in the Raman signal of explosive molecules (b) the amount of explosive molecules adsorbed on the Cu structural surface could be less compared with R6G molecules due to the dissimilar sizes of molecules (c) screening of local filed effects on freshly adsorbed explosive molecules by the possible residual R6G molecules present on the nanostructured target.

However, further detailed studies are necessary before tangible reasons are identified. From our previous studies [37] and present results we firmly believe that the Cu structures with rough edges are more compatible with R6G providing larger SERS signal and Cu nanostructured (or) periodic ripple substrates are well matched for explosive molecules for generating the enhanced Raman signal. Further improvements in SERS signal can be achieved by combining the benefits of both nanostructures and nanoparticles on a single substrate [48].

4. Conclusions

In summary, TTC–Cu–Cl, TPC–Cu–Cl colloidal solutions in TTC, TPC and Cu/CuCl nanocomposites in chloroform were prepared by means of ps laser ablation of bulk Cu target. Significant enhancements ($\sim 10^5$) in the fluorescence were obtained for TTC/TPC placed on Cu/CuCl nanocomposites compared to the case wherein fluorophores were directly adsorbed (E.F. $\sim$333) on the substrates (TTC–Cu–Cl, TPC–Cu–Cl colloids). The possible reasons behind the enhancement are deliberated in detail. Furthermore, we obtained significant Raman enhancements with Cu NSs for secondary explosives (of μM concentration), R6G (typically nM) recorded on different days. Estimated enhancement factor for R6G ($\sim 10^8$) was higher compared to that obtained for the explosive molecules ($>10^5$).

Acknowledgements

We acknowledge the financial support from DRDO, India. We acknowledge the corroles provided by Dr. Giribabu, IICT, Hyderabad.

Appendix A. Supplementary data

Supplementary data associated with this article can be found, in the online version, at doi:10.1016/j.cplett.2015.01.006.

References

[1] J. Ramos, T. Potta, O. Scheideler, K. Rege, ACS Appl. Mater. Interfaces 6 (2014) 14861.
[2] L. Kyeong-Seokm, M.A. El-Sayed, J. Phys. Chem. B 110 (2006) 19220.
[3] S. Hamad, P. Gopala Krishna, S.P. Tewari, S. Venugopal Rao, J. Phys. D: Appl. Phys. 46 (2013) 485501.
[4] P. Gopala Krishna, S. Hamad, S.P. Tewari, S. Sreedhar, M.D. Prasad, S. Venugopal Rao, J. Appl. Phys. 113 (2013) 073106.
[5] L. En-Chiang, J. Fang, P. Se-Chul, S. Thomas, J. Pezoldt, H.O. Jacobs, Adv. Mater. 25 (2013) 3554.
[6] G. Santoro, S. Yu, M. Schwartzkopf, P. Zhang, S.K. Vayalil, J.F.H. Risch, M.A. Rübhausen, M. Hernández, C. Domingo, S.V. Roth, Appl. Phys. Lett. 104 (2014) 243107.
[7] S. Botti, S. Almaviva, L. Cantarini, A. Palucci, A. Puiu, A. Rufoloni, J. Raman Spectrosc. 44 (2013) 463.
[8] J. Mbah, K. Moorer, L. Pacheco-Londoño, S. Hernandez-Rivera, G. Cruz, J. Raman Spectrosc. 44 (2013) 723.
[9] K. Kneipp, Y. Wang, H. Kneipp, L.T. Perelman, I. Itzkan, R.R. Dasari, M.S. Feld, Phys. Rev. Lett. 78 (1997) 1667.
[10] Surface-Enhanced Raman Scattering – Physics and Applications, edited by K. Kneipp, M. Moskovits, and H. Kneipp (Springer, 2006).
[11] C. Wang, et al., Appl. Phys. Lett. 100 (2012) 023107.
[12] F. Mei, X. Xiao, Z. Dai, J. Xu, Y. Zhou, C. Zhong, L. Wu, J. Appl. Phys. 114 (2013) 083523.
[13] L. Guo, C. Xing Zhang, L. Deng, G.X. Zhang, H.J. Xu, X.M. Sun, J. Appl. Phys. 115 (2014) 213101.
[14] E. Sheremet, R.D. Rodriguez, D.R.T. Zahn, A.G. Milekhin, E.E. Rodyakina, A.V. Latyshev, J. Vac. Sci. Technol. B 32 (2014) 04E110.
[15] S.D. Choudhury, R. Badugu, K. Ray, J.R. Lakowicz, J. Phys. Chem. C 116 (2012) 5042.
[16] J.R. Lakowicz, Anal. Biochem. 298 (2001) 1.
[17] J.R. Lakowicz, K. Ray, M. Chowdhury, H. Szmacinski, Y. Fu, J. Zhang, K. Nowaczyk, Analyst 133 (2008) 1308.
[18] Near-Infrared Surface-enhanced Fluorescence using Silver Nanoparticles in Solution (thesis by M.D. Furtaw), University of Nebraska, 2013.
[19] Z. Zhang, P. Yang, H. Xu, H. Zheng, J. Appl. Phys. 113 (2013) 033102.
[20] K. Saravanan, B.K. Panigrahi, R. Krishnan, K.G.M. Nair, J. Appl. Phys. 113 (2013) 033512.
[21] C.D. Geddes, J.R. Lakowicz, J. Fluoresc. 12 (2002) 121.
[22] M. Moscovits, J. Chem. Phys. 69 (1978) 4159.
[23] J.I. Gersten, A. Nitzan, J. Chem. Phys. 73 (1980) 3023.
[24] C.K. Chen, R.B.A. de Castro, Y.R. Shen, Phys. Rev. Lett. 46 (1981) 145.
[25] J.R. Lakowicz, et al., J. Fluoresc. 14 (2004) 425.
[26] R.J. Amjad, M.R. Sahar, M.R. Dousti, S.K. Ghoshal, M.N.A. Jamaludin, Opt. Exp. 21 (2013) 14282.
[27] J.R. Lakowicz, Principles of Fluorescence Spectroscopy, 3rd edn., Springer, New York, 2006.
[28] A. Kinkhabwala, Z. Yu, S. Fan, A. Yuri, K. Müllen, W.E. Moerner, Nat. Photonics 3 (2009) 654.
[29] S. Kuhn, U. Hakanson, L. Rogobete, V. Sandoghdar, Phys. Rev. Lett. 97 (2006) 017402.
[30] J. Zhang, Y. Fu, M.H. Chowdhury, J.R. Lakowicz, Nano Lett. 7 (2007) 2101.
[31] Y. Chen, K. Munechika, D. Ginger, Nano Lett. 7 (2007) 690.
[32] Y. Zhang, K. Aslan, M.J.R. Previte, C.D. Geddes, Appl. Phys. Lett. 90 (2007) 173116.
[33] S. Hamad, P.G. Krishna, S.P. Tewari, S. Venugopal Rao, Pramana-J. Phys. 82 (2014) 331.
[34] A.V. Simakin, V.V. Voronov, N.A. Kirichenko, G.A. Shafeev, Appl. Phys. A 79 (2004) 1127.
[35] T. Mortier, T. Verbiest, A. Persoons, Chem. Phys. Lett. 382 (2003) 650.
[36] S. Karolína, J. Pfleger, P. Marek, Appl. Surf. Sci. 256 (2010) 2979.
[37] S. Hamad, G. Krishna Podagatlapalli, M.A. Mohiddon, S. Venugopal Rao, Appl. Phys. Lett. 104 (2014) 263104.
[38] G. Krishna Podagatlapalli, S. Hamad, M.A. Mohiddon, S. Venugopal Rao, Appl. Surf. Sci. 303 (2014) 217.
[39] S. Venugopal Rao, G. Krishna Podagatlapalli, S. Hamad, J. Nanosci. Nanotechnol. 14 (2014) 1364.
[40] V.S. Shetti, U.R. Prabhu, M. Ravikanth, J. Org. Chem. 75 (2010) 4172.
[41] S. Hamad, S.P. Tewari, L. Giribabu, S. Venugopal Rao, J. Porphy. Phth. 16 (2012) 140.
[42] P.T. Anusha, D. Swain, T.S. Prashant, S.P. Tewari, L. Giribabu, S. Venugopal Rao, J. Phys. Chem. C 116 (2012) 17828.
[43] G. Corrado, S. Sanchez-Cortes, O. Francioso, J.V. Garcia-Ramos, Anal. Chim. Acta 616 (2008) 69.
[44] E.C. Le Ru, E. Blackie, M. Meyer, P.G. Etchegoin, J. Phys. Chem. C 111 (2007) 13794.
[45] Y. Yang, et al., Nanoscale 4 (2012) 2663.
[46] J.A. Ciezak, S.F. Trevino, Chem. Phys. Lett. 403 (2005) 329.
[47] Z.A. Dreger, Y. Tao, Y.M. Gupta, J. Phys. Chem. A 118 (2014) 5002.
[48] Z.-M. Jin, W. Gu, X.-B. Shi, Z.-K. Wang, Z.-Q. Jiang, L.-S. Liao, Adv. Opt. Mater. 2 (2014) 588.